Trehalose-6-phosphate signaling regulates lateral root formation in Arabidopsis thaliana

Stefania Morales-Herrera[a,b,c,d] (iD), Joris Jourquin[a,b] (iD), Frederic Coppé[a,b] (iD), Lorena Lopez-Galvis[a,b,c,d], Tom De Smet[e] (iD), Alaeddine Safi[a,b] (iD), Maria Njo[a,b] (iD), Cara A. Griffiths[f], John D. Sidda[g], James S. O. Mccullagh[g] (iD), Xiaochao Xue[g], Benjamin G. Davis[g,h,i] (iD), Johan Van der Eycken[e], Matthew J. Paul[f] (iD), Patrick Van Dijck[c,d,j] (iD), and Tom Beeckman[a,b,1] (iD)

Plant roots explore the soil for water and nutrients, thereby determining plant fitness and agricultural yield, as well as determining ground substructure, water levels, and global carbon sequestration. The colonization of the soil requires investment of carbon and energy, but how sugar and energy signaling are integrated with root branching is unknown. Here, we show through combined genetic and chemical modulation of signaling pathways that the sugar small-molecule signal, trehalose-6-phosphate (T6P) regulates root branching through master kinases SNF1-related kinase-1 (SnRK1) and Target of Rapamycin (TOR) and with the involvement of the plant hormone auxin. Increase of T6P levels both via genetic targeting in lateral root (LR) founder cells and through light-activated release of the presignaling T6P-precursor reveals that T6P increases root branching through coordinated inhibition of SnRK1 and activation of TOR. Auxin, the master regulator of LR formation, impacts this T6P function by transcriptionally down-regulating the T6P-degrader trehalose phosphate phosphatase B in LR cells. Our results reveal a regulatory energy-balance network for LR formation that links the 'sugar signal' T6P to both SnRK1 and TOR downstream of auxin.

trehalose-6-phosphate signaling | lateral root formation | energy-balance | SnRK1 | TOR

Modification of root systems through development of lateral roots (LRs) is vital for nutrient and water acquisition; this strongly impacts plant adaptation and indeed landscapes in diverse environments and under climate change. LRs are initiated from the pericycle LR founder cells (LRFCs) through a series of cell divisions (1) creating a primordium that grows through existing cell layers (2, 3). Diverse hormone regulators of LR formation have long been described, including brassinosteroids, ethylene, cytokinin, and auxin, the latter being recognized as the main hormonal LR regulator (4, 5). However, the integration of carbon utilization and energy into the associated regulation of plant growth and development is much less well characterized than hormone signaling.

Snf1-related protein kinase1 (SnRK1) (orthologue of AMP-activated protein kinase (AMPK)) (6) and the Target of Rapamycin (TOR) protein kinase (7) are the master regulators of carbon and energy signaling pathways in all organisms. Interaction but not regulation in planta has been demonstrated (8), as SnRK1 and TOR interact in vitro through Regulatory-Associated Protein of TOR 1B (RAPTOR1B), (9). SnRK1 inhibits energy-consuming processes (10), whereas TOR promotes carbon and energy consumption (11); hence, SnRK1 and TOR have globally antagonistic roles in plant growth and development. In plants, the pivotal sugar signal, trehalose 6-phosphate (T6P, number 12 in *SI Appendix*, Fig. S1) has been proposed to act as a plant growth regulator in diverse developmental and metabolic processes (12, 13). T6P inhibits SnRK1 (14, 15), and it has been shown that T6P-synthase (TPS) class II proteins function as negative regulators of SnRK1 (16), but nothing is known about T6P regulating TOR. Recently, LR formation during short-term energy deprivation was shown to require SnRK1 (17), and TOR has been proposed as a central gatekeeper for root branching (18). How SnRK1, T6P, and TOR could together integrate carbon and energy signaling with hormonal (auxin) signaling during LR formation is still unknown.

A Strategy for Testing T6P as a Small-Molecule Regulatory Signal in LR Growth. In this study, we investigated the role of T6P during LR formation. As LR formation is considered to be a highly energy-demanding process, we set out to identify putative connections with the energy sensors SnRK1 and TOR that can suppress and/or trigger signaling pathways, thereby contributing to LR formation. We adopted a multifaceted genetic and chemical approach for molecular modulation of signals both at the organismal and tissue level, coupled with transcriptomic and phenotypic response assessment. These included

Significance

Plants differ from animals in having an open growth strategy guaranteeing continuous growth and development after embryogenesis. Insight into the signaling networks that control growth and developmental processes in plants has increased considerably in recent decades showing the involvement of transcriptional networks and plant hormones. The open growth strategy involves the spatiotemporal formation of new organs during the entire life cycle such as new lateral roots (LRs) on the primary root axis. The decision to make a new organ requires the accommodation of energy to the right cells at the right time. Our work uncovers a tissue-specific energy balancing network during the early phase of LR formation that integrates energy with auxin signaling through the pivotal sugar signal, trehalose 6-phosphate.

tissue-targeted-CRISPR focused on ablating SnRK1 and TOR catalytic activities, coupled with use of transgenic plants with a promoter active during early LR formation at both higher (auxin response module) and lower (TOR and SnRK1 signaling) levels, as well as direct chemical perturbation with T6P and its analogues. We found that the local and specific T6P-increased levels induce LR formation from the first stage onward. Moreover, this effect requires repression of SnRK1 and promotion of TOR activities. We present evidence at multiple levels that T6P acts as an energy signal that through the inhibition of SnRK1 activity and the induction of TOR activity stimulates the formation of new LR. Furthermore, auxin interferes with T6P levels by acting upstream of trehalose phosphate phosphatase B expression in LRFCs.

Results

Expression and Functional Characterization of Trehalose Phosphate Phosphatase B (TPPB) during LR Formation. As the degrader of T6P (number 12 in *SI Appendix*, Fig. S1), TPP activities are a hallmark of T6P pathway activity in relevant tissues. A complete set of promoter-β-glucuronidase protein reporter lines was used (19) to perform a comparative analysis of all *AtTPP* expression patterns during LR development (*SI Appendix*, Fig. S2). We found that *TPPA, TPPB, TPPH,* and *TPPI* were expressed in cells of LR primordium (LRP) stages while *TPPD, TPPG,* and *TPPJ* were expressed in the tissues surrounding LR. *TPPB* was expressed from early LR formation onward, from stage I (*SI Appendix*, Fig. S2 and Fig. 1*A*), indicative for a potential key role. *TPP*-focused in silico analyses using the Visual LR Transcriptome Compendium (VisuaLRTC) (20) confirmed that *TPPB* is differentially expressed during LR formation in contrast to the other *TPPs* (*SI Appendix*, Fig. S3).

Next, to probe the effect of the removal of the TPP T6P-degrader activity, *tppb-1* and *tppb-2* seedlings from knockout and knock-down *TPPB* T-DNA insertion lines (21) (Fig. 1 *B* and *C*) were studied. Consistent with a putative role for *TPPB* and T6P, these showed higher LR branching density (22) (Fig. 1 *D* and *F*). Interestingly, in *TPPB* mutant plants, a greater density of early stages LRP was observed (Fig. 1*E*). Furthermore, to investigate whether *TPPB* function is required locally in LR cells, we generated tissue-specific CRISPR/Cas knockout (TSKO) lines (23) based on the expression of a CRISPR/Cas construct targeting *TPPB* with the promoter of *GATA23* (p*GATA23*) commanded Cas9 expression, *GATA23* is commonly used as an early LRP marker (24). Tissue-specific downregulation of *TPPB* resulted in an enhancement of LR formation in the root branching zone (Fig. 1*G*) without affecting the primary root length (*SI Appendix*, Fig. S4). In addition, we generated *TPPB* overexpressor transgenic lines (*TPPB*OE1, *TPPB*OE2, and *TPPB*OE3: Fig. 1 *B* and *C*) and found lower LR branching density (Fig. 1 *D* and *F*). Together, these results suggest that T6P levels are relevant for early LR formation and are during this process negatively controlled by *TPPB*.

Modulation of T6P Levels in Roots Controls LR Formation Triggering. Next, given the possible central role of T6P, we perturbed T6P levels in planta in multiple ways. First, we used the plant-permeable, high-intensity light (HL)-inducible T6P precursor, DMNB-T6P to directly increase T6P levels in planta, designed to mask T6P's charge and increase its hydrophobicity (25). After irradiation by HL (25), T6P generated from DMNB-T6P at levels as low as 10nM promoted the LR branching density (Fig. 2 *A* and *B*); interestingly, there are more emerged LRs in the newly formed part of the primary root ("Section III" in *SI Appendix*, Fig. S5A). Moreover, following the photoconversion

of DMNB-T6P to T6P in planta, there is a significant rise of LR density over time (Fig. 2*C* and *SI Appendix*, Fig. S5B), indicating a general promotive effect on LR formation in the root branching zone by higher T6P levels. Interestingly, direct modulation even with T6P itself was also seen, albeit at much higher concentrations (1 mM) with again, an increase in LR branching density (Fig. 2*D*) and promotion of early LR developmental stages (Fig. 2*E*) in the primary root, specifically in the root branching zone (*SI Appendix*, Fig. S6) without accelerating LRP development (*SI Appendix*, Fig. S7). In addition, we monitored the effect of T6P treatment on the establishment of "prebranch sites" (PBS), static sites of DR5:LUC expression in the primary root that contain cells that are competent to develop into future LR (26). We found that T6P promotes the establishment of PBS (Fig. 2*G*) without affecting the periodicity and amplitude in DR5:LUC oscillations in the elongation zone (*SI Appendix*, Fig. S8 *A* and *B*). At the effective T6P concentrations, 10,000 to 100,000-fold greater than required for DMNB-T6P, T6P accumulation in roots of the treated seedlings could indeed be detected (*SI Appendix*, Fig. S9), although it should be noted that this, in part, could also reflect direct cell-surface adsorption under these conditions. Consistent with a T6P-specific mechanism, using an inhibitor of trehalase: validamycin A (27) or an alternatively phosphorylated trehalose-4-phosphate (T4P) instead had no measurable effect on LR density in the root branching zone upon application (Fig. 2*F* and *SI Appendix*, Fig. S10). The T6P-driven LR induction was found to be moderated by T6P-degrader *TPPB*. Consistent with a central role for T6P, *TPPB* overexpression and knockout transgenic lines inhibited DMNB-T6P-mediated LR-induction (Fig. 2*H*). Moreover, this modification did not affect the primary root lengths (*SI Appendix*, Fig. S11).

Finally, we generated two independent p*GATA23*:*otsA* lines (Fig.3 *A* and *B*) containing the promoter of *GATA23*, fused to the coding sequence of *otsA* for the *Escherichia coli* TPS capable of promoting T6P production in planta (28). We observed that p*GATA23*:*otsA* lines displayed higher LR branching density (Fig. 3*C*). p*GATA23*:*otsA* plants also exhibit perturbation in the expression of some SnRK1 target genes (*SI Appendix*, Fig. S12A). Moreover, both lines had a higher density of non-emerged LRP as well as emerged LRs (Fig. 3*D*) without affecting primary root length (*SI Appendix*, Fig. S12B). Together, these varying modes of targeted in planta T6P generation coherently demonstrated that higher levels of T6P are sufficient and required to promote LR formation.

Energy Balance during LR Formation. It has recently been shown that SnRK1 is involved in LR formation during the acute stress of short-term energy deprivation (17) – SnRK1 is a known metabolic stress sensor (9). However, any broader fundamental role of this master kinase in the formation of an LR has not been described. In silico analyses (20) of the expression profiles of the catalytic subunits of SnRK1—KIN10 and KIN11—showed that both are regulated during LR formation (*SI Appendix*, Fig. S13A) and that notably these are down-regulated specifically in LRP cells (*SI Appendix*, Fig. S13B) based on an LR single-cell transcriptome study (29). Prompted by such an indicative link, we found that *kin10* and *kin11* mutant plants both displayed higher LR densities than wild-type in the root branching zone (Fig. 4 *A* and *C* and *SI Appendix*, Fig. S14A), while the respective overexpression lines, KINO1 and KINO2, displayed lower emerged LR densities in the root branching zone (Fig. 4 *B* and *D* and *SI Appendix*, Fig. S14B). This indicated that energy balance control of LR development relies on a low SnRK1 activity. This is supported by the generated TSKO-KIN10 lines (23) through the expression of a guide
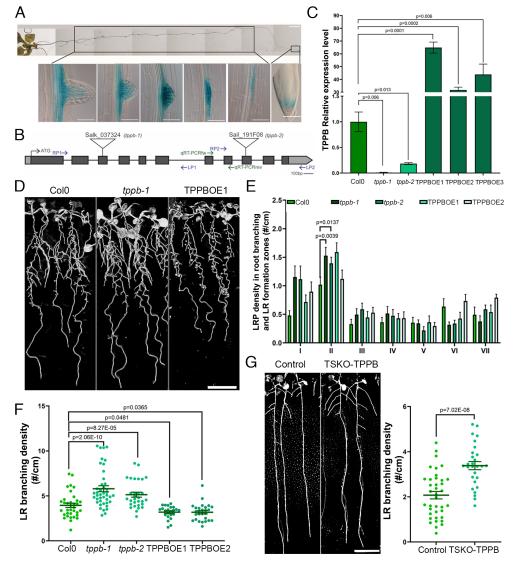
Fig. 1. Trehalose Phosphate Phosphatase B (*TPPB*), a negative regulator of LR formation. (*A*) *pTPPB:GUS* expression, 12 d after germination (DAG), insets: *TPPB* expression in the root tip and during different stages of LR development. (Scale bars, 1 mm (*Upper*) or 100 μm (*Lower*).) (*B*) Genomic *TPPB* scheme showing untranslated regions (UTRs) in light gray boxes, exons in dark gray boxes, and introns as black lines. Two Transfer DNA (T-DNA) insertion mutants (Salk_037324/*TPPB-1* and Sail _191F08/*TPPB-2*) that were isolated and primers used for genotyping (RP1 and LP1 for *TPPB-1*; RP2 and LP2 for *TPPB-2*) and for studying expression levels (qRT-PCRfw and qRT-PCRrev) are indicated on the map. (*C*) Relative *TPPB* expression levels in T-DNA and overexpression lines (*TPPB*OE1, *TPPB*OE2, and *TPPB*OE3). Presented are means ± SEM from three experimental replicates. *p*-values were obtained using one-way ANOVA. (*D*) Phenotype of 12DAG wild-type (Col0), *tppb-1*, and *TPPB*OE1 seedlings grown on vertical plates. (Scale bar, 1 cm.) (*E*) Staging of primordia in 6DAG seedlings, stages = I-VII. Bars and error bars indicate means ± SEM from two experimental replicates, n = 10 to 12 seedlings. Statistical significance was determined using a Generalized Estimation Equation (GEE) model. (*F*) Quantification of emerged LR density in root branching zone of 12DAG *TPPB* transgenic lines. Dots represent individual datapoints, and lines and error bars represent means ± SEM of three experimental replicates. n = 23 to 42 seedlings. *p*-values were calculated via Poisson regression with Dunnett's correction. (*G*) Phenotype (*Left*) and emerged LR density in root branching zone (*Right*) of 12DAG tissue-specific knockout (TSKO) T1 seedlings (TSKO-*TPPB*). Control plants represent FAST negative seedlings of this line. Individual datapoints and means±SEM are shown. n = 28 to 38 seedlings. Statistical significance was determined via Poisson regression. (Scale bar, 1 cm.)

RNA targeting KIN10 and Cas9 expression under the control of p*GATA23* (24). This TSKO-KIN10 system targeted KIN10 reduction to early LR stages including LRFCs in this way drove the formation of more LRs in the root branching zone (Fig. 4 *E* and *F* and *SI Appendix*, Fig. S14*C*). These results strongly suggested that a decrease of SnRK1 activity in early LR developmental stages (as would be caused by SnRK1 inhibitor T6P) is sufficient to achieve the necessary carbon energy balance signaling to trigger LR formation.

To evaluate the power of T6P to drive the SnRK1 signaling pathway, we again used T6P and T6P precursors directly. Additionally, we employed SnRK1-marker genes as previously identified in reference (30), whose expression profiles were shown

to be mediated by KIN10 that positively correlates with sugar and carbon deprivation. Expression analysis of validated downstream SnRK1 target genes, such as UDPGDH, TPS5, and bZIP11 (repressed by SnRK1) and ASN1 and TPS8 (induced by SnRK1) (14) in roots treated with T6P (1 mM) or light-activated precursor DMNB-T6P (10 nM under HL), respectively, showed up- and downregulation in a manner consistent with T6P inhibiting SnRK1 activity in roots (Fig. 4 *G* and *H*). Interestingly, T6P-driven LR induction apparently requires only threshold reduction of levels of SnRK1 activity since *kin10*, *kin11-1*, and *kin11-2* mutant seedlings exposed additionally to light-activated DMNB-T6P did not result in an even greater LR branching density (Fig. 4*I*). Moreover, promotion of SnRK1 activity in KINO1 and KINO2
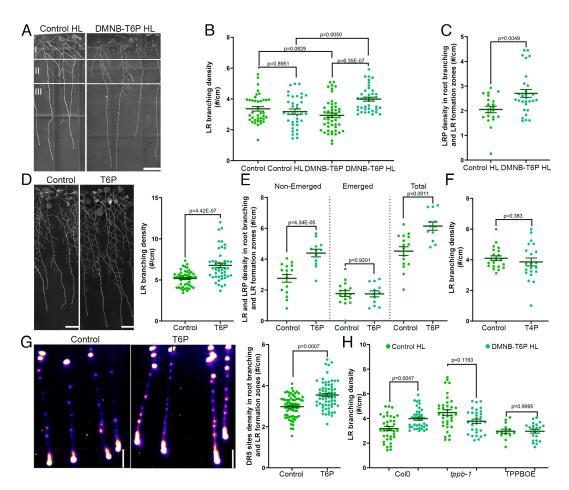
Fig. 2. T6P and DMNB-T6P treatments promote LR formation. (*A*) Phenotype of 10DAG Col0 seedlings transferred at 2DAG to control (DMSO 0.1%) or DMNB-T6P (10 nM) for 3 d and then exposed to high light (HL) treatment for 7 h followed by growth under normal conditions for 4 d. Root sections: I, root part developed before transfer. II, part developed during treatments. III, part developed after HL. (Scale bars, 1 cm.) (*B*) LR density in root branching zone of 10DAG Col0 seedlings, treated as described in *A*. The *P* value was calculated using Poisson regression with Tukey's correction (n = 36 to 48). (*C*) LRP density of 9DAG *pCYCB1;1:GUS* seedlings, treated as indicated in *A* and quantified at 3 d after high light treatment (DAHL). Poisson regression was used to calculate *P* values (n = 21 to 29). (*D*) Phenotype (*Left*) or LR density quantification in root branching zone (*Right*) of 12DAG wild-type seedlings that were transferred at 2DAG to control or T6P (1 mM). *p*-values were obtained using Poisson regression (n = 47). (Scale bars, 1 cm.) (*E*) Non-emerged, emerged, and total LRP density in root branching and LR formation zones of 8DAG Col0 seedlings, transferred at 2DAG to control or T6P (1 mM). Statistical significances were determined using a GEE model (n = 12 to 16). (*F*) LR density quantification in the root branching zone of 12DAG Col0 seedlings that were transferred at 2DAG to control or T4P (1 mM). Statistically significant differences between treatments were determined via Poisson regression (n = 21). (*G*) DR5:LUC expression in 8DAG pDR5:LUC seedlings, transferred at 2DAG to control or T6P (1 mM) (*Left*) and quantification of DR5 sites (*Right*). (Scale bar, 0.5 cm.) Statistical significance was determined via Poisson regression (n = 65 to 67). (*H*) 10DAG Col0, *TPPB*OE1, and *tppb-1* LR densities in root branching of seedlings treated as in *A*. *p*-values were calculated using Poisson regression with Tukey's correction (n = 14 to 39). Quantitative data presented as means ± SEM from three independent experiments (two for *E*).

seedlings does not allow T6P to induce LR formation in the root branching zone (Fig. 4*J*). All these phenotypes occurred without affecting primary root length (*SI Appendix*, Fig. S15)

When plants experience a low metabolic sugar status, SnRK1 is activated. On the other hand, in the high metabolic sugar status, TOR is induced and promotes growth (11). Interestingly, it is known that aspects of root architecture can be modified when TOR signaling is repressed (31), and recently, the TOR complex has been recognized as a gatekeeper for postembryonic root branching involving auxin-dependent pathways (18). Moreover, we found that expression of genes encoding for the TOR subunits RAPTOR1A and RAPTOR1B (20) is transcriptionally regulated during LR formation (*SI Appendix*, Fig. S13*A*) and, indeed, more strongly expressed in LRP cells as based on a recently reported LR single-cell transcriptome study (*SI Appendix*, Fig. S13*B*) (23). Second, using a similar tissue-specific strategy that we developed for *TPPB* and *KIN10* (see above), we generated TSKO-TOR lines and found that they displayed lower LR branching densities (Fig. 5*A* and *SI Appendix*, Fig. S16 *A* and *B*); these results are consistent with a need for a high TOR activity locally in early LR

stages including LRFCs to promote LR formation. Next, to assess whether T6P has any effect on TOR, we observed that addition of T6P slightly promoted TOR phosphorylation (Fig. 5*B*) and TOR transcription in roots (Fig. 5*C* DMNB-T6P in Fig. 5*D*). Finally, we also found that boosting T6P levels in roots was not sufficient to promote new LR biogenesis in *raptor1b* mutants nor in TOROE plants (Fig. 5*E*), again suggesting TOR interaction without affecting primary root lengths (*SI Appendix*, Fig. S17).

Auxin Regulates TPPB Expression during LR Formation. In addition, we evaluated the role of auxin, as the main regulator, in the T6P-LR induction. VisuaLRTC data suggest that *TPPB* might be repressed by auxin during early LR development in an INDOLE-3-ACETIC ACID 14 (IAA14)/SOLITARY ROOT 1 (SLR1)—AUXIN-RESPONSIVE FACTOR (ARF)7/19-dependent manner (20). This prediction was further confirmed through the analysis of *TPPB* expression in auxin-treated seedlings showing that *TPPB* was strongly down-regulated by auxin (*SI Appendix*, Fig. S18*B*), and this repression occurs in LR cells (*SI Appendix*, Fig. S18*A*). *TPPB* has an auxin-responsive element (TGTCTC, 15 bp upstream of
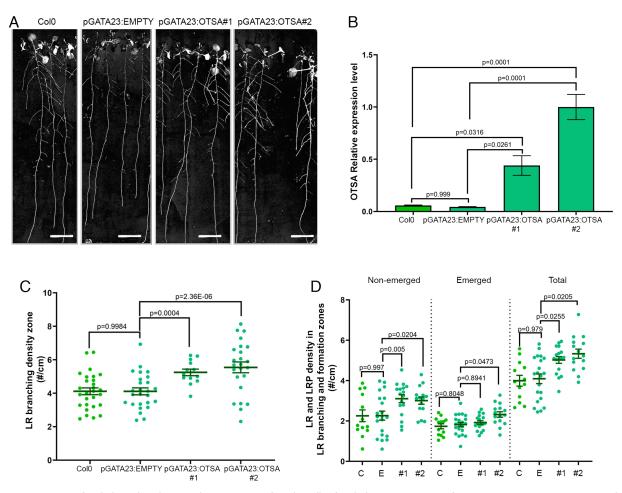
Fig. 3. Overexpression of Trehalose Phosphate Synthase (TPS) in LR founder cells of Arabidopsis promotes LR formation. *GATA23* promoter was used to drive specific expression of the *otsA* from *Escherichia coli* in LR founder cells to induce heterologous overexpression of TPS. (*A*) Phenotype of 12DAG seedlings, from left to right: Col0, plants containing the empty p*GATA23* vector (p*GATA23*:empty), p*GATA23*:otsA line#1, and p*GATA23*:otsA line#2. (Scale bars, 1 cm.) (*B*) otsA relative transcription levels in root tissue of 8DAG seedlings of Col0, p*GATA23*:empty, p*GATA23*:otsA#1, and p*GATA23*:otsA#2. The data represent three experimental replicates with three technical repeats for each. An analysis of variance (ANOVA) with a one-way design was conducted and *p*-values are indicated. (*C*) LR density in root branching zone of the plants described in *A*. Data represent three experimental replicates (n = 14 to 27). Statistically significant differences between lines were determined via Poisson regression with Tukey correction. (*D*) Nonemerged, emerged, and total densities in root branching and LR formation zones of 8DAG Col0, p*GATA23*:empty, p*GATA23*:otsA#1, and p*GATA23*:otsA#2 seedlings. Bars represent means±SEM of three experimental replicates (n = 17 to 21). *p*-values were determined using a GEE model.

the start codon) in its promoter, while the translational inhibitor cycloheximide did not block *TPPB* downregulation by auxin (*SI Appendix*, Fig. S18*D*), meaning that it might represent a direct target of auxin signaling. Moreover, this downregulation was partially reduced and abolished, respectively, in *slr1* and *arf7arf19* mutant plants (*SI Appendix*, Fig. S18*C*), thereby establishing that *TPPB* repression by auxin seems to be dependent on the IAA14/ARF7ARF19 auxin response module. This also proposes a temporally auxin-induced promotion of T6P levels at the onset of LR formation.

Together, these data suggest that T6P-driven LR induction makes use of TOR as a positive energy regulator and that the boosting effect of T6P on LR formation relies on both an inhibitory relationship with SnRK1 and a positive effect of TOR, thereby revealing the existence of an energy balancing mechanism from T6P to TOR in the process of LR formation that could be regulated by auxin (Fig. 6).

Discussion

Living organisms need to maintain cellular carbon energy homeostasis during growth and development with common carbon energy signaling mechanisms through AMPK/SnRK1 and TOR in both animals and in plants. Programming of animal stem cells depends on constraints imposed by nutrient and carbon levels (33). In plants, the entry to mitosis in stem cells is regulated by carbon levels (34). LR formation starts with auxin signaling in LRFCs that leads to a burst in proliferation as the daughter cells divide and differentiate. The strong inducing potency of auxin requires the activity of feedback mechanisms through the induction of the auxin signaling inhibitors Aux/IAAs as IAA14, IAA15, and IAA18 during the early stages of LR formation (35–37). We show here that auxin signaling down-regulates *TPPB* expression through the IAA14/ARF7ARF19 signaling module (*SI Appendix*, Fig. S18). Downregulation of *TPPB* is essential for normal LR formation as TSKO-*TPPB* and the *tppb-1* and *tppb-2* mutants promote LR development (Fig. 1). Local upregulation of T6P during early stages of LR development and the feeding of light-activable DMNB-T6P indicate that T6P is a fundamental regulator of carbon energy source for LR—it acts as the active signal possibly transmitted by the IAA14/ARF7ARF19-*TPPB* regulatory sequence in LRFCs, even though it is clear that at this stage, more research is required to confirm that this auxin module solely participates in this regulation (Fig. 6). Furthermore, how these proteins interact with trehalose metabolism genes that can impact
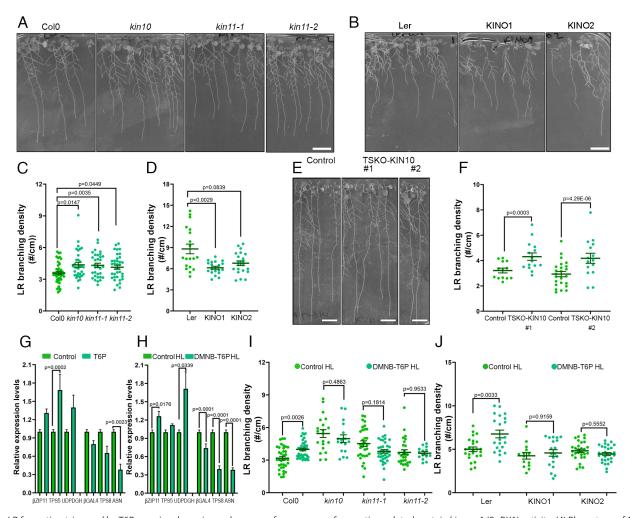
Fig. 4. LR formation triggered by T6P as a signal requires a decrease of sucrose non-fermenting-related protein kinase 1 (SnRK1) activity. (*A*) Phenotype of 12DAG seedlings of Col0, *kin10, kin11-1*, and *kin11-2* mutants. (*B*) Phenotype of Ler and overexpression lines of KIN10: KINO1 and KINO2 12 DAG seedlings grown in vertical plates. (*C*) LR density quantification in the root branching zone of seedlings in (*A*). *p*-values calculated using the Poisson regression with Dunnet's adjustments (n = 23 to 47). (*D*) LR density quantification in the root branching zone of seedlings in (*B*). Statistical significance was determined via Poisson regression with Dunnet's correction (n = 19 to 21). (*E*) Phenotype and LR density quantification in the root branching zone (*F*) of 12DAG TSKO seedlings designed to knockout specifically KIN10 in the LR founder cells using the *GATA23* promoter (TSKO-KIN10#1 and #2). Control plants represent respective FAST negative seedlings. Statistically significant differences were determined via Poisson regression (n = 13 to 24). (*G*) Relative expression of SnRK1-marker genes in root tissue of 8DAG Col0 seedlings treated for 6 d with T6P (1mM) or treated as described in Fig. 2*A*, and collected after 1 DAHL. (*H*) BZIP11, TPS5, and UDPDGH are down-regulated by SnRK1, and βGAL4, TPS8, and ASN are up-regulated by SnRK1 according to ref. 23. Data represent three experimental replicates with three technical repeats. *p*-values were obtained using the two-way ANOVA test. (*I*) Quantification of LR density in the root branching zone after four DAHL of 10DAG Col0, *kin10kin11-1*, and *kin11-2* seedlings treated as in Fig. 2*A*. Statistical significance was determined via Poisson regression with Tukey's adjustments (n = 19 to 39). (*J*) LR density in the root branching quantification after four DAHL of 10DAG Ler, KINO1, and KINO2 seedlings treated as in Fig. 2*A*. *p*-values were calculated using Poisson regression with Tukey's correction (n = 14 to 29). Quantitative data are presented as means±SEM from three independent experiments.

T6P levels has to be elucidated together with technology to reliably measure T6P specifically in LRFCs.

SnRK1 conserves carbon and energy and is a negative regulator of growth and development (14, 38). SnRK1 has been shown to prime LR initiation as a stress response after short-term low light exposure or unexpected darkness (17), but until now, it has remained unclear how the investment of new carbon required for LR formation is integrated into SnRK1 function. We found that lower SnRK1 activity enhances LR branching, which is in line with lower expression of *KIN10* during the last steps of LR formation (*SI Appendix*, Fig. S13*A*) and with resistance to LR-inhibition by ABA shown in SnRK1 *sesquiα2-1* and *sesquiα2-2* mutants (39). It has been established that T6P inhibits SnRK1 to promote growth and development and that T6P/SnRK1 regulates hundreds of genes (14, 28, 38) while recently TPS class II proteins were shown to act as negative regulators of SnRK1 (16). Here, we showed that T6P treatments result in changes of expression of

genes previously associated with SnRK1 (30) and T6P (40), supporting the idea that T6P-regulated LR development relays through SnRK1. The requirement for SnRK1 inhibition during the early stages of LR development is supported by the local knockout of SnRK1 using the TSKO system (Fig. 4 *E* and *F*).

As in animals and yeasts, TOR apparently acts antagonistically to SnRK1 in plants as well (11, 41). Both protein kinases are energy sensors that according to metabolic status can adjust metabolism and/or gene expression to change growth. Our results suggest that T6P positively regulates TOR (Fig. 5). The results propose the existence of antagonistic roles between SnRK1 and TOR during LR formation. T6P engages both TOR positively and SnRK1 negatively to drive energy regulation for LR formation (Fig. 6). Our work shows that T6P is a fundamental sugar signal necessary for LR formation. Moreover, the study provides a paradigm for how a single pivotal sugar signal (T6P) can link the hormone auxin to carbon and energy signaling through the
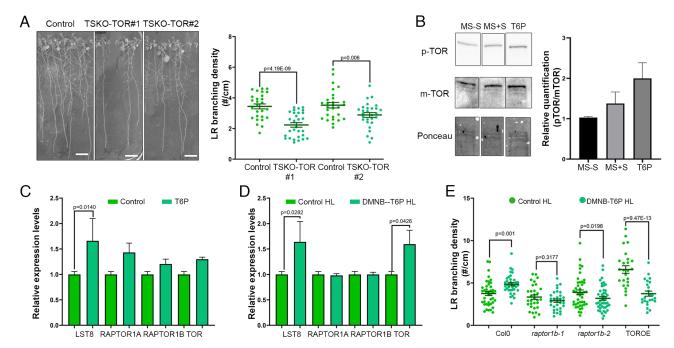
Fig. 5. LR formation promoted by T6P relies on an increase of Target of Rapamycin (TOR) activity. (*A*) Phenotype (*Right*) and LR density quantification in the root branching zone of 12DAG control and TSKO-TOR#1 and #2 plants (*Left*), designed as indicated in 1G. *p*-values were calculated using Poisson regression (n = 27 to 29). (*B*) Phosphorylation assay of TOR using the Phospho-mTOR antibody (TOR-P, 289 KDa) after T6P (1 mM) treatment. Positive control is 0.5XMS with sucrose (MS+S) and negative control 0.5XMS without sucrose (MS-S). The membranes were reblotted with mTOR antibody. Ponceau staining was used as a protein loading control. The *Right* shows the quantification of three experimental replicates. (*C*) Relative expression of TOR-complex genes (LST8, RAPTOR1A, RAPTOR1B, and TOR) in root tissue of 8DAG Col0 seedlings treated for 6 d with T6P (1 mM) or as is described in Fig. 2*A* after one DAHL (*D*). Data represent means ± SEM of three experimental replicates with three technical repeats. *p*-values were obtained using two-way ANOVA. (*E*) Emerged LR density at four DAHL of 10DAG Col0, *raptor1b* mutants, and TOROE seedlings treated as in Fig. 2*A*. Statistical significance was determined via Poisson regression applying Tukey's corrections (n = 24 to 43). Quantitative data are presented as means ± SEM from three experimental replicates.

antagonistic master regulators SnRK1 and TOR to initiate new organ growth.

Materials

Arabidopsis thaliana was used as a model plant in this work. The ecotypes Columbia 0 (Col0) and Landsberg erecta (Ler) were used as WT lines, and the following mutants were obtained from the mentioned authors or stock centra: *slr-1* (35)*, arf7arf19* Arabidopsis Biological Resource Center (ABRC), CS24629 (42), *tppb-1* (SALK_037324), *tppb-2-2* (SAIL_191F08) (21), *kin10* (ABRC, CS69182), *kin11-1* (ABRC, CS69183), *kin11-2* (ABRC, CS69184), KINO1 (ABRC, CS69185, Ler background), KINO2 (ABRC, CS69186, Ler background) (ref. 16, KIN10 and KIN11 lines were characterized in ref. 37), TOROE (G548(7)), *raptor1b-1* (SALK_101990), and *raptor1b-2* (SALK_022096) (43). All the mutants were genotyped using the specific primers according to the T-DNA Primer Designed Tool (http://signal.salk.edu/tdnaprimers.2.html) (*SI Appendix*, Table S1). *TPPB*OE1, *TPPB*OE2, and pTP-P::GUS lines were described in ref. 19. pCycB1;1::GUS Col0 background (44) was used as a mitotic activity reporter line. We used the line pDR5:LUC (Col0 background) (26) as a reporter of prebranching sites.

All the accession numbers used in this research are in *SI Appendix*, Table S2.

Methods

Plant Growth Conditions. Seeds from different lines were sterilized by a chlorine-gas method (45), sown, and germinated in square plates that contain 0.5× Murashige and Skoog (MS) salt mixture medium with MES (0.5 g/L), Myo-inositol (0.1 g/L), and solidified with Phytoagar (8 g/L) or Phytagel (6 g/L) in the case of DMNB-T6P treatment. Seeds were stratified in a dark room at 4 °C for 48 h, and then, plates were put vertically in the in vitro culture room under continuous light (100 μmol/m^{2}s^{-1}) at 22 °C until investigation.

Histochemical and Histological Analysis. For detailed analysis of TPP expression during LR formation, the available developmental stages in roots at six DAG of pTPP::GUS seedlings were analyzed. β-glucuronidase(GUS) staining assays were performed as described in ref. 46. After 24 h, the reaction was stopped,

and the seedlings were mounted on glass microscopy slides in 90% lactic acid (Merck) to clear the tissue for inspection of primordia. Detailed staging of LRs was done as described in ref. 1. Samples were examined by differential interference contrast microscopy (BX53; Olympus).

Compound Treatments. For NAA treatments, 6 DAG of pTPPB::GUS or five DAG Col0, *slr-1* and/or *arf7arf19* seedlings were transferred to 0.5XMS solid medium without sucrose supplemented with 10 μM NAA and 0.1% DMSO in control plates. For Cycloheximide (CHX) treatments, 5 DAG Col0 seedlings were treated for 2 h with 10 μM NAA or control (0 μM NAA, DMSO) and pretreated 30 min with 50 μM CHX. Trehalose (Tre) and Validamycin A (Val) treatments performed by transferring 2 DAG Col0 seedlings to 0.5XMS solid medium without sucrose supplemented with or without Trehalose dihydrate (10 μM, 100 μM, 1 mM, or 10 mM from a 130 mM stock solution diluted in water, Sigma-Aldrich) and/or Val (10 μM from a 10 mM stock solution diluted in water, Sigma-Aldrich). For the T6P or T4P treatments, 2 DAG Col0 seedlings were transferred to plates with 0.5XMS solid medium without sucrose supplemented with or without trehalose 6(or 4)-phosphate dipotassium salt (1 mM from 100 mM stock solution in water) synthesized in the Department of Biotechnology, Centre for Synthetic Biology, Ghent University, Ghent, Belgium.

DMNB-T6P Treatment. DMNB-T6P was synthesized according to previous methods (25). 2DAG Col0, Ler, *TPPB-1*, *TPPB*OE1, *kin10*, *kin11-1*, *kin11-2*, KINO1, KINO2, *raptor1b-1*, *raptor1b-2*, TOROE, and *pCYCB1;1*::GUS seedlings were transferred to 0.5XMS solid medium without sucrose containing 10 nM of DMNB-T6P dissolved in DMSO and with 0.1%DMSO used as control. The seedlings were grown for 3 d under these treatments in standard growth conditions. After treatment, half of the plates from both conditions were exposed to HL treatments (600 μmol/m^{2}s^{-1}) for 7 h. Then, the plates were returned to normal growth conditions until analysis. DAHL was used to identify the effect of the DMNB-T6P to T6P conversion on root growth.

DR5:LUCIFERASE Assays. To quantify the prebranching sites, we used 2DAG pDR5:LUC seedlings that were transferred to T6P 1 mM in 0.5XMS solid medium for 6 d. The seedlings were sprayed with 1 mM D-Luciferin (Duchefa Biochemie) solution [D-Luciferin dissolved in 0.01% (v/v) Tween80 and 0.1% (v/v) DMSO].
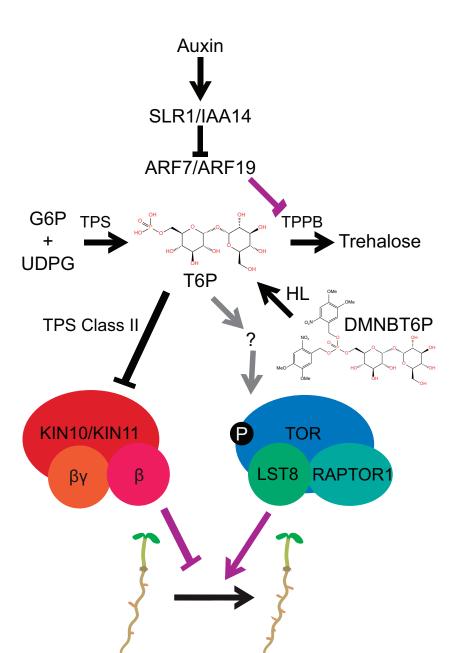
Fig. 6. T6P regulates LR growth at the center of a regulatory hub linking auxin with energy homeostasis through SnRK1 and TOR. *TPPB* is required for LR formation and is transcriptionally regulated by auxin through IAA14-ARF7/19 which down-regulates *TPPB* expression. T6P regulates LR formation through SnRK1 and TOR which are inhibited and activated, respectively, by T6P. Black lines represent links validated by previous work (16, 17, 25, 32), gray lines represent potential mechanistic links proposed here based on our own research, and purple lines links indicate relationships for which we did find genetic evidence.

Then, they were kept in darkness for 10 min to allow the appropriate absorption of D-Luciferin by the roots (47). Emitted luminescence was captured using ANDOR iKon-M 934 charge-coupled device (CCD) camera (Oxford Instruments) paired with a fixed lens (Spacecom 43F2409M-MP C 4/3" 24 mm F0.9) over a 20-min exposure time. Bright-field images of the roots were taken in each condition to be able to measure the primary roots and quantify the density of DR5:LUC sites. *DR5:LUC* oscillation frequencies and amplitudes were determined via 22-h time-lapse assays. 3DAG seedlings were transferred to plates with or without 1mM T6P, sprayed with 1 mM D-luciferin, and incubated in the dark for 1 h. Next, emitted luminescence was captured every 15 min with a 10-min exposure time using a NightSHADE LB985 in vivo plant imaging system (Berthold technologies) equipped with a deep-cooled slow scan CCD camera and the accompanying lens (Andor Instruments). Based on these time-lapses, the amplitude of and period between oscillation peaks in the oscillation zone were determined using ImageJ.

Molecular Cloning. To generate the p*GATA23*::*otsA* transgenic line, Gateway Technology (Invitrogen) was used. Genomic DNA was extracted from *E.coli* (strain K12) using the alkaline lysis method. Q5® High-Fidelity DNA Polymerase (NEB) and the primers indicated in *SI Appendix*, Table S3 were used to amplify the *otsA* gene and then cloned in the pDONR221 donor vector. p*GATA23* was available

already in the entry vector pEN-L4-p*GATA23*-R1 generated in ref. 17. Gateway LR recombination reaction was performed using pK7m24GW2 as a destination vector, obtained from the VIB Gateway vectors database (https://gatewayvectors.vib.be/). Then, Col0 plants were transformed with the final expression clones by *Agrobacterium tumefaciens* via floral dip method (48). T1 transformant seeds were selected by sowing them in 0.5XMS solid medium supplemented with 50µg/mL Kanamycin. Then, the resistant seeds were transferred to Jiffy-7 pellets® and grown in a greenhouse until the T2 generation.

Quantification of LR Formation. The number of emerged LR was quantified in each seedling using an M165C binocular microscope (Leica). We determined the LR densities in the root branching zone according to ref. 22. To perform LR staging, the protocol indicated in ref. 1 was followed. Then, LR stages were identified and counted using an Olympus BX53 DIC microscope with a x400 magnification. During the microscopic analysis, the start of the LR formation and branching zones were marked on the slides. To measure the root lengths of the root branching zone and LR formation zone, the plugin NeuronJ (49) of Fiji software was used to analyze digital images obtained from scanning the square plates with EPSON expression 11000 XL flatbed scanner. To determine the effect of T6P on the speed of LRP development, a bending assay was performed in which LR development

was initiated via gravistimulation. 5DAG seedlings were transferred to medium with or without 1mM T6P and gravistimulated (90° counterclockwise rotation). At different time points after gravistimulation, 30 treated and untreated seedlings were collected and cleared for 30 min using a chloral hydrate solution (5M chloral hydrate, 3% HCl). Next, the developmental stage of the LRP in each root bend was determined using an Olympus BX53 DIC microscope.

Gene Expression Analysis. Total RNA was extracted from root tissue using the ReliaPrep™ RNA Tissue Miniprep System (Promega) according to the manufacturer's instructions. cDNA was prepared from 1 µg of total RNA with the qScript® cDNA SuperMix (Quantabio). Gene expression was quantified using SYBR® Green Mix (Roche) mediating a RT-qPCR in a LightCycler® 480 (Roche). cDKA1;1 and EEF1α4 were used as housekeeping genes to analyze *TPPB* expression in transgenic lines and treatments. Relative expression levels in T6P/DMNB-T6P treatments, TOR, p*GATA23*:otsA#1, p*GATA23*:otsA#2, p*GATA23*:Empty, TSKO-KIN10#1, TSKO-TOR#1, and TSKO-TOR#2 transgenic lines were normalized using UBI10 and PP2A as reference genes. All reactions were performed in triplicates, and a total of three biological replicates (two for TSKO lines) were analyzed per sample. Primers used are listed in *SI Appendix*, Table S4.

TSKO Design. The gRNAs were designed using the web tool CRISPOR.org (50) to target *TPPB*, KIN10, and TOR kinase catalytic sites (Primers are enlisted in *SI Appendix*, Table S4). Then, a single gRNA was inserted in the TSKO destination vector pFASTR-p*GATA23*-Cas9-P2A-mCherry-G7T-AtU6-BsaI-CmR-ccdB-BsaI-gRNA scaffold generated as in ref. 23. For primers, see *SI Appendix*, Table S5. Following this, Arabidopsis plants were transformed by floral dip using *A. tumefaciens* with the destination vector including the designed gRNA (48). Next, the FASTR-positive seeds from T1 were selected by red fluorescence detection under a Leica M165FC fluorescence stereomicroscope. They were sown in 0.5XMS solid medium without sucrose and checked under the Leica SP8X confocal microscope for the presence of Cas9-mCherry in early stages of LR. The positives for Cas9-mCherry were transferred to jiffy and grown in a greenhouse. Lines that showed a 3:1 segregation FASTR positive:negative were selected for further propagation to generate a T3 population and to analyze their phenotype.

TOR Phosphorylation Assays. 6DAG Col0 seedlings were used. The seedlings were pretreated for 1h in 0.5XMS liquid medium without sucrose. Then, 1 mM T6P or 15 mM sucrose was added to the medium for 20 min. Next, the seedlings were collected in liquid nitrogen. Plant material was ground and extracted as indicated in ref. 51. Protein total amount in the samples was quantified using the Qubit protein assay kit (ThermoFisher). Thirty micrograms of total protein per sample was loaded, and phospho-mTOR (Ser2448) antibody (#2971, 1:1,000, Cell Signaling Technology) was used to detect TOR phosphorylation. Then, the membranes were stripped using a 1:1 (v/v) 10% SDS and 100mM glycine–HCl (pH 2.5) solution. Next, the membranes were reblotted with mTOR antibody (#2,972, 1:1,000, Cell Signaling Technology). Horseradish peroxidase–conjugated anti-rabbit was used as secondary antibody and visualized using Western Lightning Plus ECL (PerkinElmer). The ChemiDoc XRS+ imaging system (Bio-Rad) was used to visualize the blots. To quantify the pTOR signal, the band intensity was measured with ImageLab software (v.6.0.0, Bio-Rad) and then normalized by the mTOR signal in each treatment.

Synthesis of Trehalose-6-Phosphate Dipotassium Salt Trihydrate (T6P) and Trehalose-4-Phosphate Dipotassium Salt Tridecahydrate (T4P). Triethylamine (11.6 mL, 83.1 mmol) was added to a stirred solution of PCl$_3$ (2.27 mL, 26 mmol) in diethyl ether (160 mL) at 0 °C. A solution of compound **4** (2.6 g, 2.6 mmol) in diethyl ether (100 mL) was added. The resulting reaction mixture was stirred for 30 min at 0 °C and then at room temperature. After 24 h, it was cooled to 0 °C, and benzyl alcohol (16.2 mL, 156 mmol) was added. Stirring was continued for 30 min at 0 °C and then for 4 d at room temperature. Pyridine (25.1 mL, 312 mmol) and acetic anhydride (14.7 mL, 156 mmol) were added, after which the reaction mixture was stirred for 24 h. Subsequently, H$_2$O$_2$ (30% aq, 26 mL) was added, followed by stirring for 24 h. The reaction mixture was then cooled to 0 °C, and Na$_2$S$_2$O$_3$ (10% aq, 260 mL) was added. After stirring for 30 min at 0 °C, the mixture was transferred to a separation funnel containing H$_2$O (250 mL). The organic phase was separated, after which the aqueous layer was extracted with CH$_2$Cl$_2$ (2 × 250 mL). The combined organic layers were dried over Na$_2$SO$_4$. After filtration, concentration in vacuo, and partial purification by flash column

chromatography (gradient elution: hexane/EtOAc 100/0 to 60/40), compound **5** was yielded as a mixture with tribenzyl phosphate. This mixture was dissolved in THF (26 mL). Tetra-n-butylammonium fluoride (1M in THF, 7.8 mL, 7.8 mmol) was added, followed by stirring overnight. The reaction mixture was transferred to a separation funnel containing KHSO$_4$ (1M in H$_2$O, 250 mL). The aqueous layer was extracted with EtOAc (3 × 250 mL). The combined organic layers were dried over anhydrous Na$_2$SO$_4$. After filtration, concentration in vacuo, and flash column chromatography (gradient elution: hexane/EtOAc 60/40 to 40/60), compound **6** was obtained (1.3 g, 1.2 mmol, 44%). To a solution of **6** (574 mg, 0.502 mmol) in MeOH (5 mL) and EtOAc (2 mL), palladium on carbon (10%, 53 mg, 0.050 mmol) was added. A balloon containing H$_2$ gas was attached to the flask. The reaction mixture was stirred at room temperature for 2 d under H$_2$ atmosphere, and subsequently filtered over celite and concentrated in vacuo, affording trehalose-6-phosphate as a white powder in a quantitative yield (212 mg, 0.502 mmol). To a solution of trehalose-6-phosphate (212 mg, 0.502 mmol) in H$_2$O (20 mL), KOH (0.05 M in H$_2$O, 20.1 mL) was added. The mixture was subjected to lyophilization, giving compound **7** (trehalose-6-phosphate dipotassium salt trihydrate) as a white powder in quantitative yield (278 mg). Compound **11** was obtained from **10** in a similar reaction procedure as for compound **5**. Compound **12** was afforded via the general procedure described for the synthesis of compound **7**. For additional details, see *SI Appendix, Supplementary Materials and Methods*.

T6P Measurements. 5DAG Col0 seedlings were transferred to liquid 0.5XMS without sucrose as control or supplemented with 1 mM T6P for 3 d incubated in normal growth conditions and at harvest washed in distilled water three times for 15 min each time. Then, the root tissue was collected, weighed, stored at −70 °C, and ground to a fine powder in liquid nitrogen. T6P was extracted as in ref. 52. Ten microliters of each sample was loaded into a Dionex UltiMate 3,000 LC System (Thermo Scientific) equipped with a C-18 column (Acquity UPLC -HSS T3 1.8 µm; 2.1 × 150 mm, Waters) coupled to a Q Exactive Orbitrap mass spectrometer (Thermo Scientific) operating in negative ion mode. A step gradient was carried out using solvent A (10 mM TBA and 15 mM acetic acid) and solvent B (100% methanol). The gradient started with 5% of solvent B and 95% of solvent A and remained at 5% B until 2 min after injection. A linear gradient to 37% B was carried out until 7 min and increased to 41% until 14 min. Between 14 and 26 min, the gradient increased to 95% of B and remained at 95% B for 4 min. At 30 min, the gradient returned to 5% B. The chromatography stopped at 40 min. The flow was kept constant at 0.25 mL/min, and the column was placed at 40 °C throughout the analysis. The MS operated in full scan mode [m/z range: (70.0000 to 1050.0000)] using a spray voltage of 4.80 kV, capillary temperature of 300 °C, sheath gas at 40.0, and auxiliary gas at 10.0. The AGC target was set at 3.0E + 006 using a resolution of 140,000, with a maximum IT fill time of 512 ms. Data collection was performed using the Xcalibur software (Thermo Scientific). Data analysis was performed by integrating the peak areas (El-Maven–Polly–Elucidata). The T6P concentration was normalized with the fresh weight of each sample.

Statistical Analysis. Statistical analyses were performed in R (53) or SAS (version 9.4 of the SAS System for Windows). For LR branching and DR5:LUC site density data, a Poisson model (or a quasi-Poisson model in case of overdispersion) was fitted to the LR or DR5:LUC site counts, with genotype and/or treatment (and if applicable their interaction) as fixed effects. A log-link function was applied, and log-transformed primary root lengths were used as an offset variable. LR numbers were analyzed in the same way without the use of an offset variable. Statistical analyses of primary root lengths were performed via an ANOVA or a Kruskal–Wallis rank-sum test as a nonparametric alternative, with genotype and/or treatment (and if applicable their interaction) as fixed effects. Where applicable, post hoc Tukey and Dunnett's tests were set up using the "emmeans" package (54). In those cases where root lengths were only compared between two conditions, as well as for the comparison of *DR5:LUC* oscillation frequencies and amplitudes, two-tailed Student's *t* tests or Mann–Whitney tests (nonparametric alternative) were performed. For the analysis of LR developmental stages, a GEE model was fitted to the primordium count rate with genotype and developmental stage, as well as their interaction, as fixed effects using a log-link function and selecting a Poisson distribution. Log-transformed root lengths were used as an offset. The correlations between the counts were modeled as exchangeable correlations. At each stage, we tested whether there was an equal primordium count rate in the mutant or treatment compared with the appropriate control. The analysis was done with

the genmod procedure (in SAS). Contrast statements were set up with the plm procedure using the lsm estimate statement. To correct for multiple testing, the maxT procedure was used as implemented in the plm procedure. To determine statistical differences between the proportions of LRP at certain developmental stages in gravistimulation-induced root bends in control or T6P-treated seedlings, Chi-square tests were performed.

Data, Materials, and Software Availability. All study data are included in the article and/or *SI Appendix*.

Author affiliations: [a]Department of Plant Biotechnology and Bioinformatics Ghent University, Ghent B-9052, Belgium; [b]Vlaams Instituut voor Biotechnologie Center for Plant Systems Biology, Ghent B-9052, Belgium; [c]Laboratory of Molecular Cell Biology, Katholieke Universiteit Leuven, Leuven B3001, Belgium; [d]Vlaams Instituut voor Biotechnologie-Katholieke Universiteit Leuven Center for Microbiology, Leuven B3001, Belgium; [e]Department of Organic and Macromolecular Chemistry, Laboratory for Organic and Bio-Organic Synthesis, Ghent University, Ghent B-9000, Belgium; [f]Department of Sustainable Soils and Crops, Rothamsted Research, Harpenden AL5 2JQ, United Kingdom; [g]Department of Chemistry, Chemistry Research Laboratory, University of Oxford, Oxford OX1 3TA, United Kingdom; [h]Next Generation Chemistry, The Rosalind Franklin Institute, Didcot OX1 3TA, United Kingdom; [i]Department of Pharmacology, University of Oxford, Oxford OX1 3TA, United Kingdom; and [j]Katholieke Universiteit Leuven Plant Institute, Katholieke Universiteit Leuven, Leuven B3001, Belgium

1. J. E. Malamy, P. N. Benfey, Organization and cell differentiation in lateral roots of Arabidopsis thaliana. *Development* **124**, 33–44 (1997).
2. K. Swarup *et al.*, The auxin influx carrier LAX3 promotes lateral root emergence. *Nat. Cell Biol.* **10**, 946–954 (2008).
3. A. Jenkins *et al.*, A spatial accommodation by neighboring cells is required for organ. *Science* **343**, 178–183 (2014).
4. H. Fukaki, M. Tasaka, Hormone interactions during lateral root formation. *Plant Mol. Biol.* **69**, 437–449 (2009).
5. J. G. Dubrovsky *et al.*, Auxin acts as a local morphogenetic trigger to specify lateral root founder cells. *Proc. Natl. Acad. Sci. U.S.A.* **105**, 8790–8794 (2008).
6. A. Dahiya, R. Saini, H. S. Saini, A. Devi, Sucrose metabolism: Controls the sugar sensing and generation of signalling molecules in plants. *J. Pharmacogn. Phytochem.* **6**, 1563–1572 (2017).
7. D. Deprost *et al.*, The Arabidopsis TOR kinase links plant growth, yield, stress resistance and mRNA translation. *EMBO Rep.* **8**, 864–870 (2007).
8. A. González, M. N. Hall, S. C. Lin, D. G. Hardie, AMPK and TOR: The yin and yang of cellular nutrient sensing and growth control. *Cell Metab.* **31**, 472–492 (2020).
9. E. Nukarinen *et al.*, Quantitative phosphoproteomics reveals the role of the AMPK plant ortholog SnRK1 as a metabolic master regulator under energy deprivation. *Sci. Rep.* **6**, 31697 (2016).
10. C. Polge, M. Thomas, SNF1/AMPK/SnRK1 kinases, global regulators at the heart of energy control? *Trends Plant Sci.* **12**, 20–28 (2007).
11. T. Dobrenel *et al.*, TOR signaling and nutrient sensing. *Annu. Rev. Plant Biol.* **67**, 261–285 (2016).
12. C. M. Figueroa, J. E. Lunn, A tale of two sugars: Trehalose 6-phosphate and sucrose. *Plant Physiol.* **172**, 7–27 (2016).
13. F. Fichtner, J. E. Lunn, The role of trehalose 6-phosphate (Tre6P) in plant metabolism and development. *Annu. Rev. Plant Biol.* **72**, 737–760 (2021).
14. Y. Zhang *et al.*, Inhibition of SNF1-related protein kinase1 activity and regulation of metabolic pathways by trehalose-6-phosphate. *Plant Physiol.* **149**, 1860–1871 (2009).
15. D. W. Lawlor, M. J. Paul, Source/sink interactions underpin crop yield: The case for trehalose 6-phosphate/SnRK1 in improvement of wheat. *Front. Plant Sci.* **5**, 1–14 (2014).
16. J. Van Leene *et al.*, Mapping of the plant SnRK1 kinase signalling network reveals a key regulatory role for the class II T6P synthase-like proteins. *Nat. Plants* **8**, 1245–1261 (2022).
17. P. Muralidhara *et al.*, Perturbations in plant energy homeostasis prime lateral root initiation via SnRK1-bZIP63-ARF19 signaling. *Proc. Natl. Acad. Sci. U.S.A.* **118**, 1–10 (2021).
18. M. Stitz *et al.*, TOR acts as a metabolic gatekeeper for auxin-dependent lateral root initiation in Arabidopsis thaliana. *EMBO J.* **42**, 1–19 (2023).
19. L. Vandesteene *et al.*, Expansive evolution of the trehalose-6-phosphate phosphatase gene family in Arabidopsis. *Plant Physiol.* **160**, 884–896 (2012).
20. B. Parizot, B. de Rybel, T. Beeckman, VisualLRTC: A new view on lateral root initiation by combining specific transcriptome data sets. *Plant Physiol.* **153**, 34–40 (2010).
21. J. M. Alonso *et al.*, Genome-wide insertional mutagenesis of Arabidopsis thaliana. *Science* **301**, 653–657 (2003).
22. J. G. Dubrovsky, B. G. Fordeb, Quantitative analysis of lateral root development: Pitfalls and how to avoid them. *Plant Cell* **24**, 4–14 (2012).
23. W. Decaestecker *et al.*, CRISPR-TSKO: A technique for efficient mutagenesis in specific cell types, tissues, or organs in Arabidopsis. *Plant Cell* **31**, 2868–2887 (2019).
24. B. De Rybel *et al.*, A novel Aux/IAA28 signaling cascade activates GATA23-dependent specification of lateral root founder cell identity. *Curr. Biol.* **20**, 1697–1706 (2010).
25. C. A. Griffiths *et al.*, Chemical intervention in plant sugar signalling increases yield and resilience. *Nature* **540**, 574–578 (2016).
26. M. A. Moreno-Risueno *et al.*, Oscillating gene expression determines competence for periodic arabidopsis root branching. *Science* **1306**, 1306–1311 (2010).
27. J. Müller, T. Boller, A. Wiemken, Effects of validamycin A, a potent trehalase inhibitor, and phytohormones on trehalose metabolism in roots and root nodules of soybean and cowpea. *Planta* **197**, 362–368 (1995).
28. H. Schluepmann, T. Pellny, A. Van Dijken, S. Smeekens, M. Paul, Trehalose 6-phosphate is indispensable for carbohydrate utilization and growth in Arabidopsis thaliana. *Proc. Natl. Acad. Sci. U.S.A.* **100**, 6849–6854 (2003).
29. H. P. Gala *et al.*, A single-cell view of the transcriptome during lateral root initiation in Arabidopsis thaliana. *Plant Cell* **33**, 2197–2220 (2021).
30. E. Baena-González, F. Rolland, J. M. Thevelein, J. Sheen, A central integrator of transcription networks in plant stress and energy signalling. *Nature* **448**, 938–942 (2007).
31. B. Li *et al.*, PRR5, 7 and 9 positively modulate TOR signaling-mediated root cell proliferation by repressing tandem zinc finger 1 in Arabidopsis. *Nucleic Acids Res.* **47**, 5001–5015 (2019).
32. Y. Okushima, H. Fukaki, M. Onoda, A. Theologis, M. Tasaka, ARF7 and ARF19 regulate lateral root formation via direct activation of LBD/ASL genes in Arabidopsis. *Plant Cell* **19**, 118–130 (2007).
33. N. Shyh-Chang, H. H. Ng, The metabolic programming of stem cells. *Genes Dev.* **31**, 336–346 (2017).
34. X. Skylar, A. Sung, F. Hong, J. Chory, J. Wu, Metabolic sugar signal promotes Arabidopsis meristematic proliferation via G2. *Dev. Biol.* **351**, 82–89 (2011).
35. H. Fukaki, S. Tameda, H. Masuda, M. Tasaka, Lateral root formation is blocked by a gain-of-function mutation in the solitary-root / IAA14 gene of Arabidopsis. *Plant J.* **29**, 153–168 (2002).
36. T. Uehara, Y. Okushima, T. Mimura, M. Tasaka, Domain, II mutations in crane / IAA18 suppress lateral root formation and affect shoot development in Arabidopsis thaliana. *Plant Cell. Physiol.* **49**, 1025–1038 (2008).
37. S. H. Kim *et al.*, A gain-of-function mutant of IAA15 inhibits lateral root development by transcriptional repression of LBD genes in Arabidopsis. *Front. Plant Sci.* **11**, 1–11 (2020).
38. C. Nunes *et al.*, The trehalose 6-phosphate/snRK1. Signaling pathway primes growth recovery following relief of sink limitation. *Plant Physiol.* **162**, 1720–1732 (2013).
39. B. Belda-Palazón *et al.*, A dual function of SnRK2 kinases in the regulation of SnRK1 and plant growth. *Nat. Plants.* **6**, 1345–1353 (2020).
40. C. Nunes *et al.*, Inhibition of SnRK1 by metabolites: Tissue-dependent effects and cooperative inhibition by glucose 1-phosphate in combination with trehalose 6-phosphate. *Plant Physiol. Biochem.* **63**, 89–98 (2013).
41. E. Baena-González, J. Hanson, Shaping plant development through the SnRK1–TOR metabolic regulators. *Curr. Opin. Plant Biol.* **35**, 152–157 (2017).
42. Y. Okushima *et al.*, Functional genomic analysis of the auxin response factor gene family members in Arabidopsis thaliana: Unique and overlapping functions of ARF7 and ARF19. *Plant Cell* **17**, 444–463 (2005).
43. M. A. Salem *et al.*, RAPTOR controls developmental growth transitions by altering the hormonal and metabolic balance. *Plant Physiol.* **177**, 565–593 (2018).
44. P. C. G. Ferreira *et al.*, Developmental expression of the Arabidopsis cyclin gene cyc1At. *Plant Cell* **6**, 1763–1774 (1994).
45. B. E. L. Iii, I. Rivero, C. S. Calhoun, E. Grotewold, J. Brkljacic, Standardized method for high-throughput sterilization of Arabidopsis seeds. *J. Vis. Exp.* **128**, 1–7 (2017).
46. T. Beeckman, G. Engler, An easy technique for the clearing of histochemically stained plant tissue. *Plant Mol. Biol. Report.* **12**, 37–42 (1994).
47. W. Xuan *et al.*, Long-term in vivo imaging of luciferase-based reporter gene expression in Arabidopsis roots. *Methods Mol. Biol.* **1761**, 177–190 (2018).
48. S. J. Clough, A. F. Bent, Floral dip: A simplified method for Agrobacterium-mediated transformation of Arabidopsis thaliana. *Plant J.* **16**, 735–743 (1998).
49. M. U. C. E. Meijering, M. Jacob, J.-C.F. Sarria, P. Steiner, H. Hirling, Design and validation of a tool for neurite tracing and analysis in fluorescence microscopy images. *Cytometry* **58**, 167–176 (2004).
50. J. Concordet, M. Haeussler, CRISPOR: Intuitive guide selection for CRISPR / Cas9 genome editing experiments and screens. *Nucleic Acid Res.* **46**, 242–245 (2018).
51. J. Jourquin *et al.*, Two phylogenetically unrelated peptide-receptor modules jointly regulate lateral root initiation via a partially shared signaling pathway in Arabidopsis thaliana. *New Phytol.* **233**, 1780–1796 (2022).
52. J. E. Lunn *et al.*, Sugar-induced increases in trehalose 6-phosphate are correlated with redox activation of ADPglucose pyrophosphorylase and higher rates of starch synthesis in Arabidopsis thaliana. *Biochem. J.* **397**, 139–148 (2006).
53. R Core Team, *R: A Language and Environment for Statistical Computing* (R Foundation for Statistical Computing, Vienna, Austria, 2020).
54. R. V. Length, emmeans: Estimatedmarginalmeans, aka least-squares means. *R Package* **1**, 7 (2021).